공학석사 학위논문

Needle steering scheme within limited DOFs for MR-guided breast needle intervention robot

MR 유도 유방 바늘 중재시술 로봇을 위한

한정된 자유도 안에서 바늘 스티어링 전략

2017년 2월

서울대학교 대학원

기계항공공학부

이 정 환

Abstract

The MR-guided needle-based procedure is commonly performed for breast diagnosis and treatment. Accurate needle tip placement is important for the success of the procedure, because misplacement of the needle tip can lead to unsuccessful treatment and misdiagnosis. In addition, developing a needle steering robotic system with high precision and dexterity is required to avoid important organs, minimizing patients' trauma. However, due to the strong magnetic field and relatively small MRI bore size, developing a high degrees of freedom (DOFs) robotic system is challenging. This work proposes a needle steering scheme that can be effectively utilized in an MR-guided breast needle intervention robot under limited space of MRI bore with minimizing system size increase. To overcome the space limitation and avoid critical structures in front of the lesion, a pivot is used to change the needle insertion direction. We devise the needle pivoting breast plate to increase needle tip's DOFs and an estimation model of the needle deflection with a pivoted super-elastic flexible needle made of Nitinol. This computational model is based on large deflection beam theory and is employed for robot control. Open-loop needle targeting experiments under infrared tracking cameras are performed to verify the proposed scheme. The average targeting error and the standard deviation is 4.42 ± 2.58 mm.

Keyword: MR−guided breast needle intervention robot, Needle pivoting breast plate, Needle Steering, Super−elastic flexible needle, Needle deflection estimation, Large deflection beam theory

Student Number: 2013−23084

Table of Contents

List of Tables

List of Figures

Chapter 1. Introduction

Breast cancer is the most frequently diagnosed cancer and is the second leading cause of cancer death after lung cancer. [1] Needle-based procedures are the most common clinical interventions for breast cancer and are used for biopsy, brachytherapy, and ablation. [2, 3] Because misdiagnosis or unsuccessful treatment might occur due to the misplacement of the needle tip, accurate needle tip placement is critical for procedure's success rate. Image-guided needle intervention is performed to improve the needle tip placement accuracy. Since Magnetic Resonance Image (MRI) can provide superior soft tissue contrast without harmful ionizing radiation, it has recently gained popularity. [4, 5] Constrained by the limited space of the MRI scanner bore, breast needle intervention is currently performed outside of the MRI bore and based on MR images. Repeated needle insertion is required to locate needle tip at the desired position, and such "Trial and error"-based needle insertion may increase positioning errors and cause patients undue trauma. Hence, a precise multiple degrees of freedom (DOFs) robot is required so that the patients can remain inside the MRI bore and accurate needle tip placement can be achieved. This will allow the avoidance of multiple iterations and minimize positioning errors during needle intervention. [6, 7]

One promising robotic technology is robotic needle steering. [8] Increasing a needle tip's DOFs allows a clinician to maneuver around obstacles towards areas that are unreachable for rigid needles. There are various approaches to making steerable needles. Some of studies have used smart materials such as shape memory alloys and optic fiber to bend the needle tip. [9, 10, 11, 12] Several research teams have utilized the flexible needle's natural bending abilities inside soft tissue to steer the needle. [13, 14, 15] All of these approaches accompany additional actuators or complex components to make high DOFs needle tip motions.

Moreover, the relatively small MRI bore size, generally 70 cm in diameter, and the presence of the strong magnetic field means that there are limits on material selection and the overall system size. These limitations mean that developing a high DOFs robotic needle steering system remains a challenge. Therefore, more efficient ways of steering a needle is required to enhance the needle tip's DOFs under limited conditions.

This paper suggests a needle steering scheme that can be utilized in an MR-guided breast needle intervention robot with limited conditions, such as inside MRI bore. The needle is steered by a pivot with modifying commercial breast needle intervention device, such as a breast compressing plate. Because a pivot is the easiest way to change needle tip direction and commercial beast compressing plate can work as pivot points with little shape changes, pivots are utilized in needle steering schemes. Figure 1 shows basic concept of a pivot. This work also presents the estimation model of the needle defection with a pivoted super−elastic flexible needle made of Nitinol for robot control. This estimation model is based on the large beam deflection theory and shows the relationship between the desired insertion angle and robot position.

This paper is organized as follows: The materials used in this work are described in Section 2. Section 3 presents the needle steering method. Experimental results for the evaluation of the proposed method are given in Section 4, and the discussion is presented in Section 5.

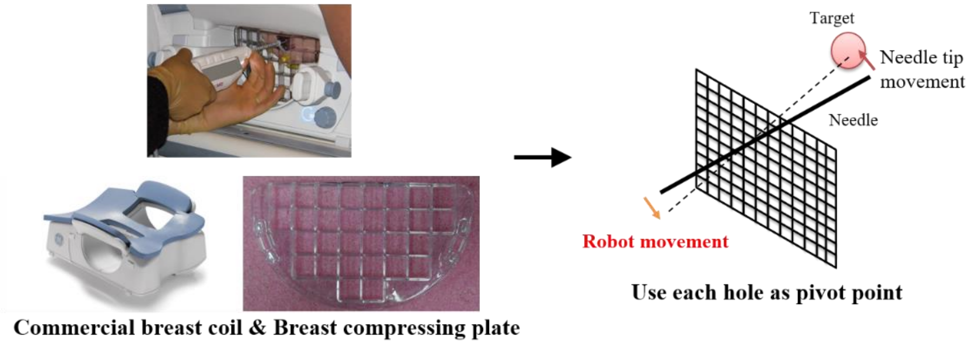

Figure 1. Concept of a pivot

Chapter 2. Materials

2.1. MR-guided breast needle intervention robot system

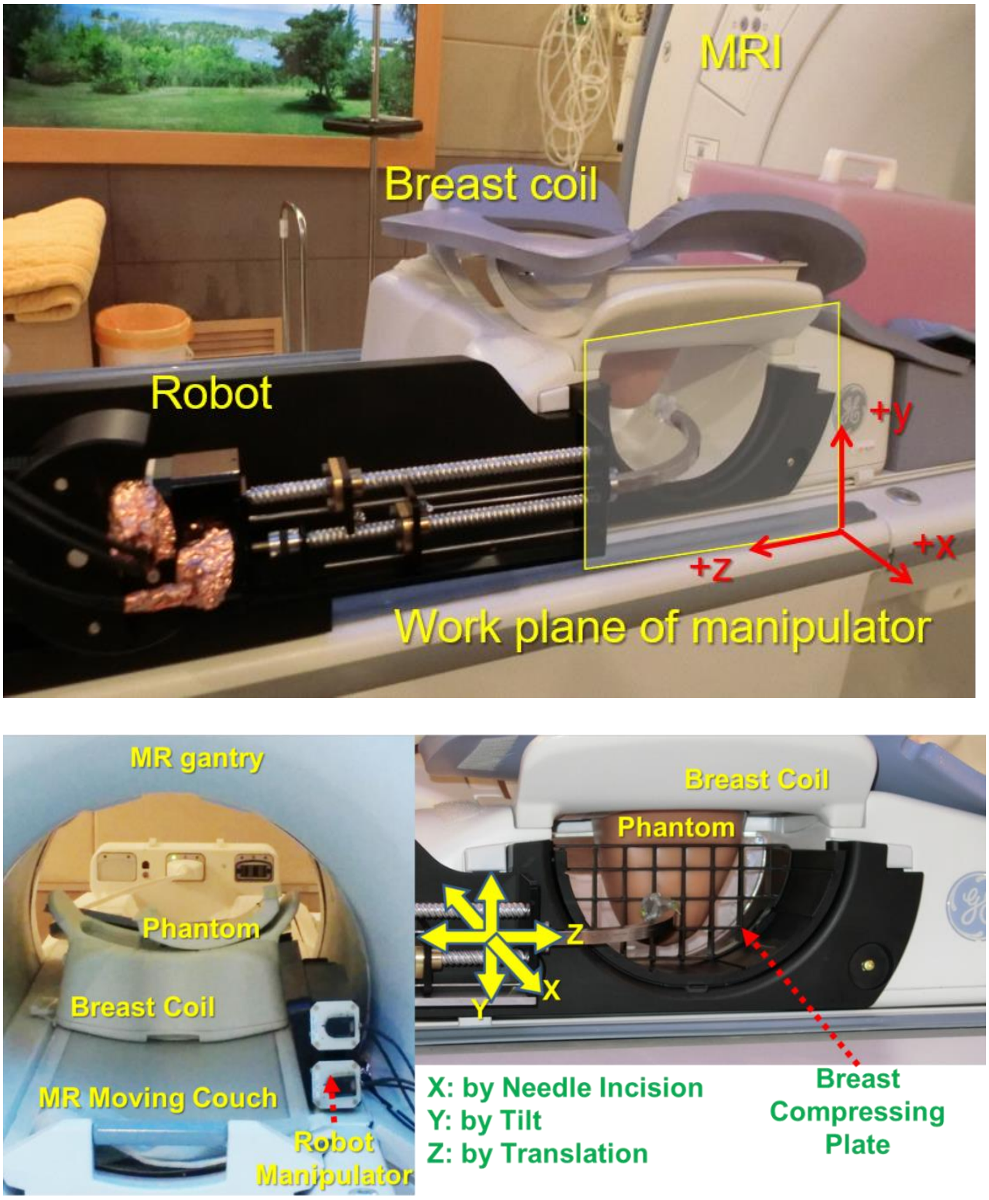

Figure 2. Developed MR-guided breast needle intervention robot (National Cancer Center, South Korea) It had 3+1 DOFs with the bendable needle approach. [16]

An MR–guided breast needle intervention robot developed by the National Cancer Center in South Korea was used in this work. [16] (Figure 2)

This robot is designed to be placed inside an MRI bore and operated therein under continuous MRI guidance. The robot can be attached to a commercial breast coil (GE, Germany), and this feature allows the robot to be located beside the patient. This design was intended to overcome the space limitation.

This robot is consisted of two main drivers for manipulator and pre–curved end effector. A manipulator to hold and move the pre–curved end effector was designed with a 2 DOFs sliding mechanism with two spindles. The end effector slides in the Z direction while two spindles drive in the same direction. A linear slider in the center holds the end effector with a pivot. Therefore, when the upper spindle and lower spindle move in different directions, the end effector tilts. With this 2 DOFs sliding mechanism, the end effector, in this case the needle exit point, is positioned on the plane parallel to the patient's sagittal plane (Y–Z plane).

Since this robot system located beside patient, needle direction should have to change 90° for insertion. The 90° direction change in the pre–curved end effector necessitates flexibility and super–elasticity characteristics. Therefore, a super–elastic Nitinol tube is chosen because its recovery characteristic without permanent deformation after bending.

The pre−curved end effector also has two spindle motors that can move the needle driver and pusher driver separately. These two spindle motors can make needle' s back and forth motion. In addition, concentric dual needles, which can be utilized in many needle intervention procedures such as biopsy, inserting a marker seed and a drug capsule, can be applied in this robot.

In short, developed MR−guided breast needle intervention robot has total 3 + 1 DOFs motion including 2 DOFs manipulator motion and 1 + 1 DOFs needle sliding (1 for inner needle and the other for outer needle). With this 3 DOFs robot motion, this robot system can send the needle point anywhere inside breast. However, this robot can not avoid obstacles inside the breast because needle insertion direction is only perpendicular to the patient' s sagittal plane (Y−Z plane). For avoiding obstacles inside breast, additional movement of needle should have to generate. To make needle' s extended movement such as steering, we utilize the needle pivoting breast plate.

2.2. Needle pivoting breast plate

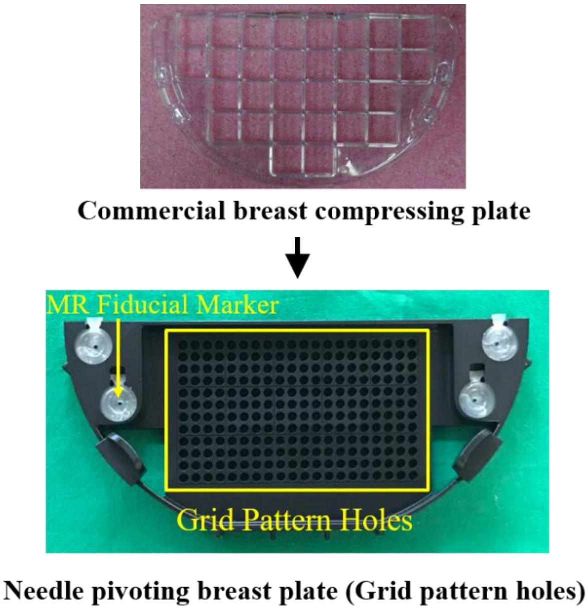

Figure 3. Needle pivoting breast plate (Grid pattern)

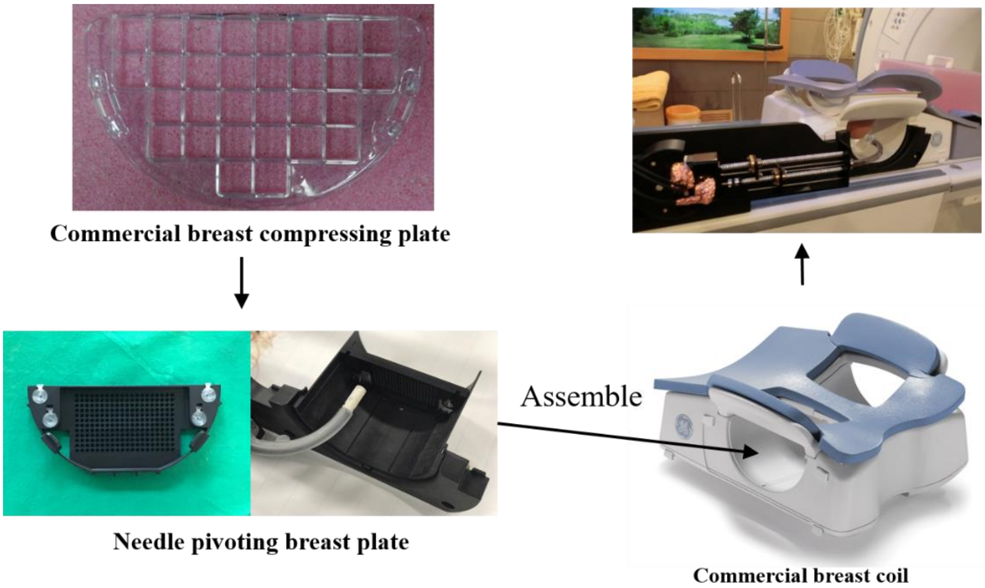

Figure 4. Overall commercial breast coil and needle pivoting breast plate

We devised a pivot grid plate to increase needle tip's DOFs. Since we utilized a bendable Nitinol needle, it was possible to change the needle direction only with pivot holes without increasing the actuators. A commercial breast compressing plate was modified to make pivot points, and 2.0 mm diameter holes were arranged in a 5.0mm grid pattern. (Figure 3) We named it the needle pivoting breast plate. This customized part is able to be directly applied in conventional MRI devices. (Figure 4) Each hole works as an initial positioning guidance. With the known position of each hole acquired by coordinate registration from the MR fiducial marker set attached to the needle pivoting breast plate, the needle can be positioned at each hole with precision. And then, each hole also works as a pivot point, we could make additional 2 DOFs needle direction change with no additional actuator.

Figure 5. shows extended robot motion with a pivot. The robot system with the needle pivoting breast plate can generate total 5 + 1 DOFs motion (1 + 1 DOF needle sliding, 2 DOFs manipulator, and 2 DOFs needle tip motion). Additional 2 DOFs needle tip motion is made by original 2 DOFs manipulator of developed robot. This extended DOFs can locate needle tip anywhere inside the breast and make various needle insertion directions. Multiple needle insertion directions have a potential to utilize in mechanism avoiding important

tissues in front of the lesion.

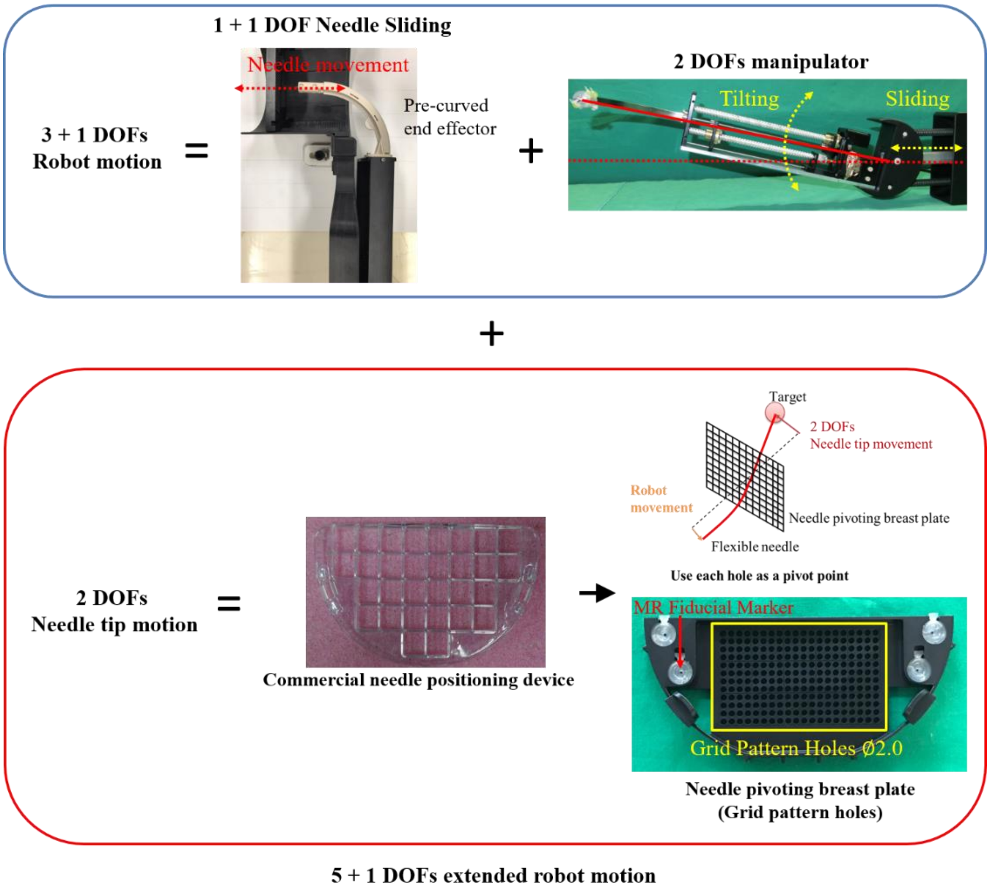

Figure 5. Extended robot motion by a pivot

Chapter 3. Methods

3.1. Needle steering procedure

The needle steering procedure using a pivot is comprised of the following steps: (1) Initial positioning of the desired needle pivoting breast plate’s hole; (2) Compute the needle insertion angle for the target position; (3) Estimate the robot’s future position to determine the desired insertion angle; (4) Move to the future position; (5) Needle insertion. (Figure 6)

There are two assumptions in robot control. First, the needle has linear elasticity, which is a basic assumption of the large beam deflection theory that is used to estimate the robot future position. Second, the needle insertion path is straight. In this approach, the needle’s natural deflection inside the tissue is negligible because of the needle’s high rigidity.

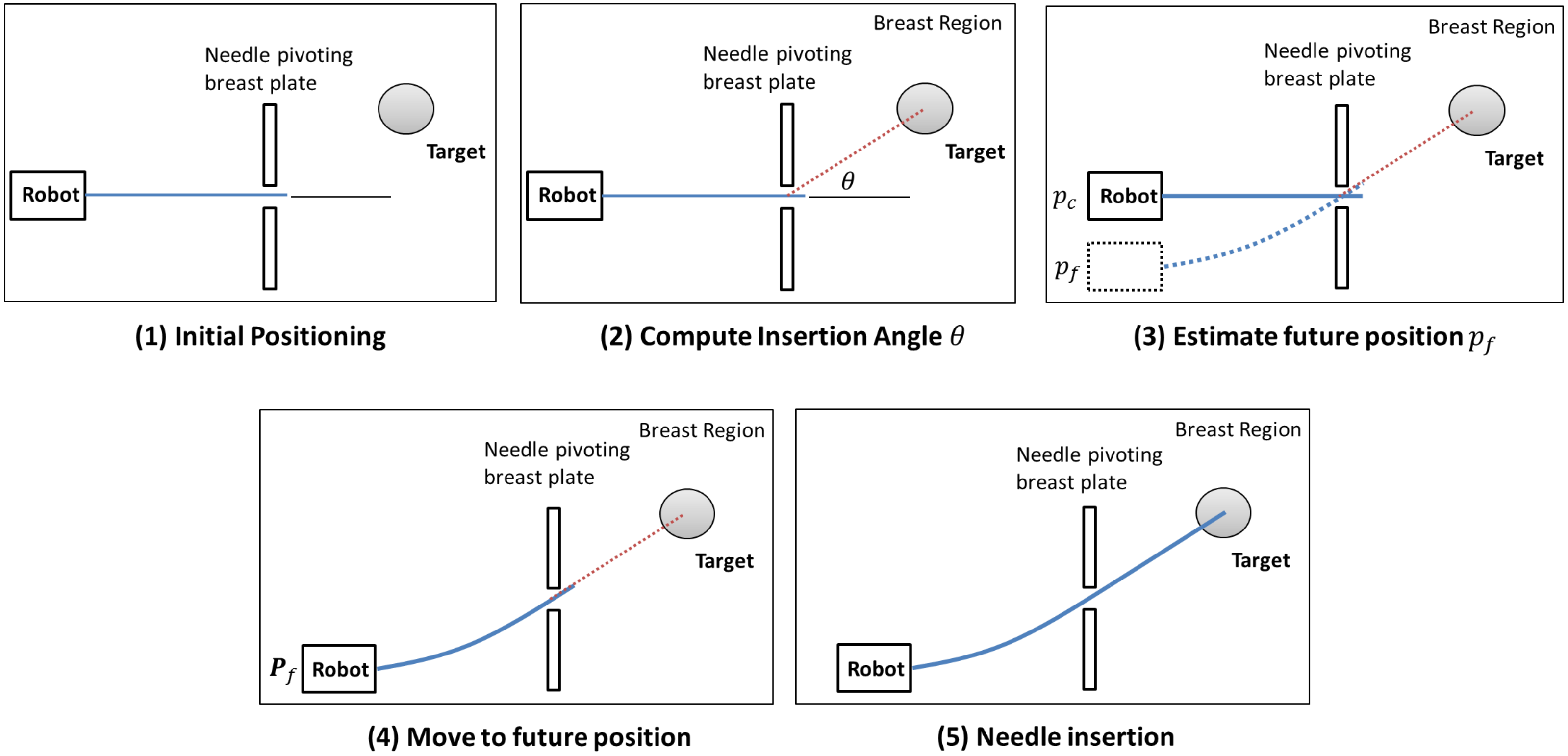

Figure 6. Needle steering procedure; (1) Initial positioning; (2) Compute the insertion angle; (3) Estimate the future position; (4) Move to the future position; (5) Needle insertion

3.2. Robot pose estimation

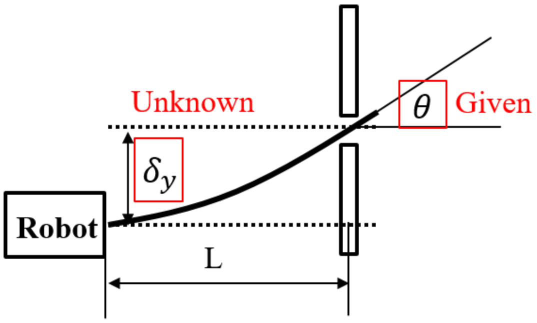

Figure 7. Schematic of the steering with the flexible needle

During the steering, the robot movement is directly transferred to the needle tip position. If the needle is rigid without deformation, estimating the robot pose is quite simple. However, this system uses a flexible needle that can induce bending during the steering. Determining a more accurate future robot position that can make a straight needle insertion path to the target requires estimating such needle deformation. Therefore, the relationship between the needle tip direction θ and the needle deflection δ_y caused by the robot's movement is required to estimate the robot's future position. (Figure 7)

3.2.1. Large deflection beam theory

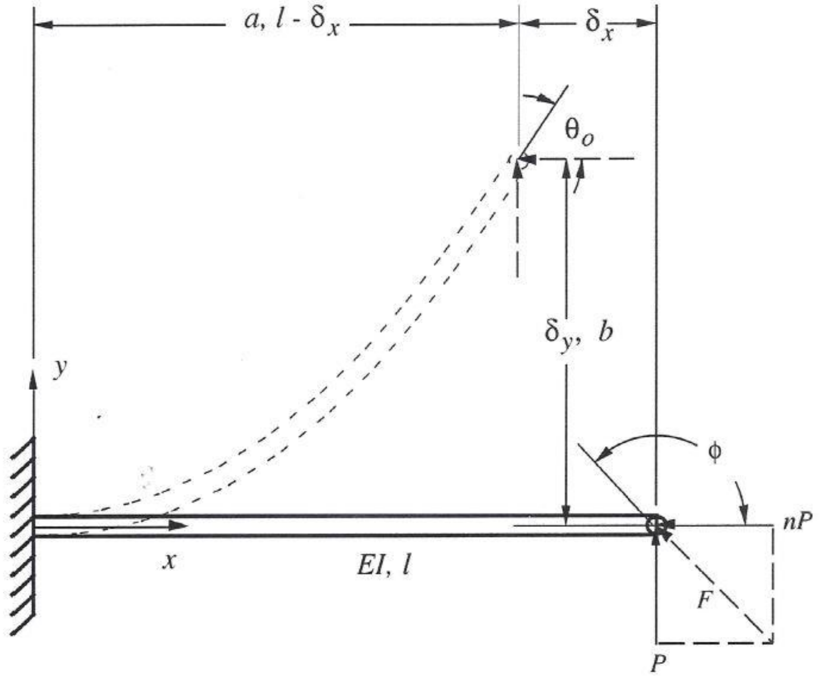

Figure 8. Large deflection of cantilever beam [18]

For computing a future robot position for steering procedure, we had to estimate the quantity of the needle deflection by the pivot. The needle deflection can be derived from the cantilever beam deflection model. Since our application showed large bending deformation, we choose the Large beam deflection theory based on the Euler−Bernoulli beam model to establish the needle deflection estimation model.

The deflection of a cantilever beam under loading can be described by the relationship between the curvature at any point on the beam and the applied moment at that point under the assumption that the beam' s material remains linearly elastic. This relationship is [17, 18]

$$\kappa = \frac{d\theta}{ds} = \frac{M}{EI} \qquad (1)$$

where $\frac{d\theta}{ds}$ is the curvature of the beam and the rate of change of θ with respect to s. E is the modulus of elasticity for the material and I is the moment of inertia for the cross-sectional area of the beam. The internal moment at any point in the beam is given by

$$M = P(a - x) + nP(b - y) \qquad (2)$$

where a is the horizontal distance from the fixed end to the free end and b is the vertical distance of the free end from its undeflected position. n is the ratio of the horizontal force to the vertical force. $(0 \leq n \leq 1)$ Substituting equation (1) to equation (2) yields

$$\kappa = \frac{d\theta}{ds} = \frac{P}{EI}[(a - x) \; + n(b - y)] \qquad (3)$$

By differentiating equation (3) once with respect to s, we obtain

$$\frac{d\kappa}{ds} = \frac{d^2\theta}{ds^2} = \frac{P}{EI}(-\frac{dx}{ds} - n\frac{dy}{ds}) \qquad (4)$$

If dx, dy and ds are infinitesimal, we can express $\frac{dx}{\mathrm{ds}}$ and $\frac{dy}{\mathrm{ds}}$ as $cos\theta$ and $sin\theta$. Therefore, equation (4) can be expressed as follow

$$\frac{d^2\theta}{ds^2} = \frac{-P}{EI}(n\ \ sin\theta + cos\theta) \qquad (5)$$

The second order differential equation (5) for θ is

$$\frac{d^2\theta}{ds^2} = \frac{d}{ds}(\frac{d\theta}{ds}) \qquad (6)$$

By the chain rule, equation (6) can be written as

$$\frac{d}{ds}\left(\frac{d\theta}{ds}\right) = \frac{d}{d\theta}(\frac{d\theta}{ds})\frac{d\theta}{ds} \qquad (7)$$

By substituting curvature $\kappa = \frac{d\theta}{ds}$ to equation (7), we obtain

$$\frac{d^2\theta}{ds^2} = \frac{d\kappa}{d\theta}\kappa \qquad (8)$$

Equation (8) can be modified as follow

$$\frac{d^2\theta}{ds^2} = \frac{d}{d\theta}(\frac{\kappa^2}{2}) \quad (9)$$

After substituting equation (9) to equation (5) and integrating, we obtain

$$\int d\left(\frac{\kappa^2}{2}\right) = \int \frac{-P}{EI}(n\ \ sin\theta + cos\theta)d\theta \quad (10)$$

Equation (10) is solved as

$$\frac{\kappa^2}{2} = \frac{P}{EI}(n\ \ cos\theta - sin\theta) + C_1 \quad (11)$$

where C_1 is integral constant. According to the figure 8, boundary conditions are $s = l$, $\theta = \theta_0$ and $\frac{d\theta}{ds} = \kappa = 0$. Therefore, integral constant C_1 is derived as

$$C_1 = \frac{P}{EI}(sin\theta_0 - n\ \ cos\theta_0) \quad (12)$$

By substituting equation (12) to equation (11), we obtain

$$\kappa = \frac{d\theta}{ds} = \sqrt{2\frac{P}{EI}(sin\theta_0 - n\ \ cos\theta_0 - sin\theta + n\ \ cos\theta)} \qquad (13)$$

Let us assume that the horizontal force does not apply at the free end ($n = 0$). Thus, equation (13) can be written as

$$\kappa = \frac{d\theta}{ds} = \sqrt{2\frac{P}{EI}(sin\theta_0 - sin\theta)} \qquad (14)$$

Equation (14) is also expressed as

$$ds = \sqrt{\frac{EI}{2P}}\frac{d\theta}{\sqrt{(sin\theta_0 - sin\theta)}} \qquad (15)$$

Where $\frac{dy}{\mathrm{ds}} = sin\theta$, equation (15) is re−written as

$$dy = \sqrt{\frac{EI}{2P}}\frac{sin\theta}{\sqrt{(sin\theta_0 - sin\theta)}}d\theta \qquad (16)$$

Integrating both side and substituting the angle at the free end θ_0 to θ yields

$$\delta_y = y(\theta_0) = \sqrt{\frac{EI}{2P}}\int_0^{\theta_0}\frac{sin\theta}{\sqrt{(sin\theta_0 - sin\theta)}}d\theta \qquad (17)$$

δ_y is the vertical deflection at the free end. The final equation can be utilized in the estimation of the robot' s future pose.

3.2.2. Estimation of external force

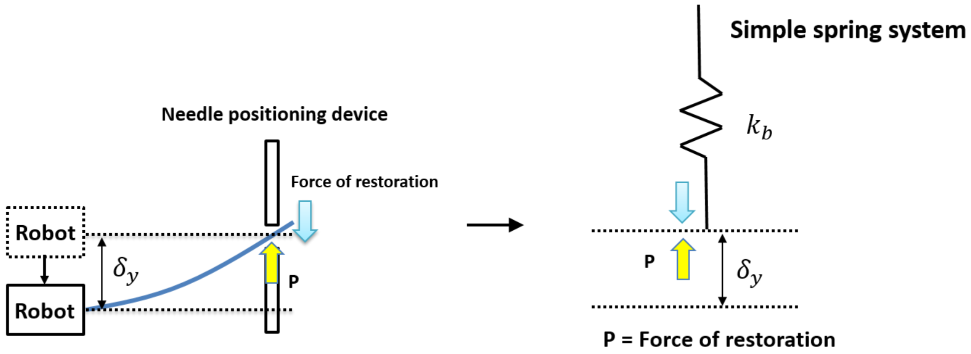

Figure 9. Approximated simple spring system

Equation (17) shows the vertical deflection at the free end when an external force is applied. However, deflection is induced by robot base movement in this robot system. Thus, the external force P in equation (17) is an unknown variable. The bending of the needle can be regarded as a simple spring model to estimate the external force P. (Figure 9) The resistance of a member against bending deformation, the bending stiffness k_b, works as a spring constant in this spring model. Thus, the restoration force applies at the pivot point. The external force at the pivot point can be substituted for the force of restoration. Then, the external force can be written as

$$P = k_b \delta_y \qquad (18)$$

k_b is the bending stiffness and δ_y is the deformation due to the robot’ s position change. Substituting equation (18) into equation (17) allows us to write δ_y as

$$\delta_y = \sqrt[3]{\frac{EI}{2k_b}A^2} \qquad (19)$$

$$where\ \ A = \int_0^{\theta_0} \frac{sin\theta}{\sqrt{(sin\theta_0 - sin\theta)}} d\theta$$

3.2.3. Measurement of bending stiffness

Bending stiffness is one of the material’ s unique properties in equation (19). Figure 10 shows the typical loading and unloading behavior of a super−elastic Nitinol tube. The linear elastic behavior is shown and bending stiffness k_b can be measured within the range shows linear elastic behavior under particular deformation. However, the bending stiffness also changes the length from the fixed end to the point of application. Thus, characterizing the bending stiffness with respect to the length of the needle is necessary to acquire the bending stiffness at an arbitrary pivot point.

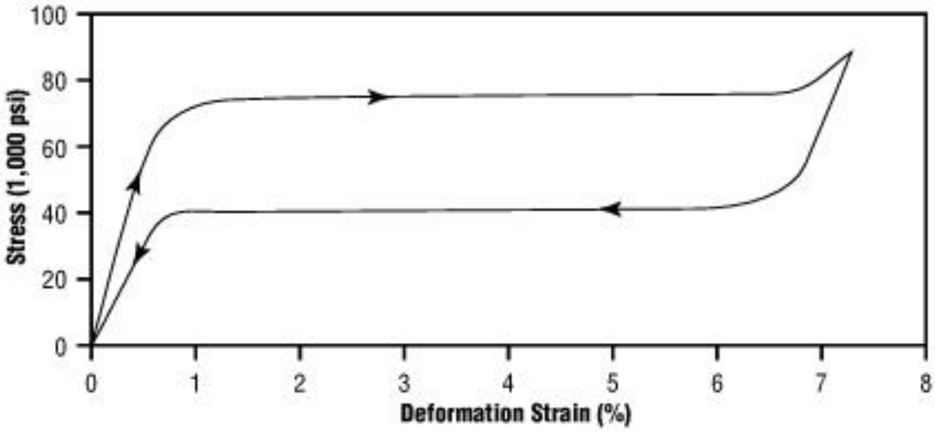

Figure 10. Typical Loading and Unloading Behavior of Super−elastic Ni−Ti [19]

The measurement setup, composed of the force gauge (AFG−2, Axis Sensitive Co. Ltd., South Korea), a digital caliper (CD−10CPX, Mitutoyo, Japan) and concentric dual Nitinol needle, is shown in Figure 11. The dimension of the needles is presented in Table 1. We measured the force of restoration with respect to the change in needle length and deflection. Figure 12 shows the measurement results in three−dimensional space.

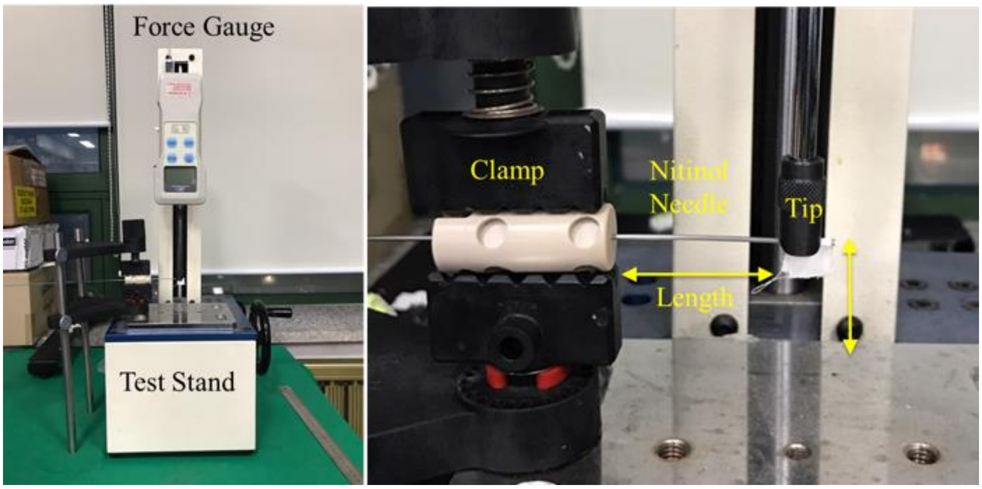

Figure 11. Setup for measuring the needle bending stiffness

	Outer needle	Inner needle
Elastic modulus (GPa)	75	75
OD (mm)	1.270	0.7176
ID (mm)	0.838	0.413

Table 1. Nitinol needle specification

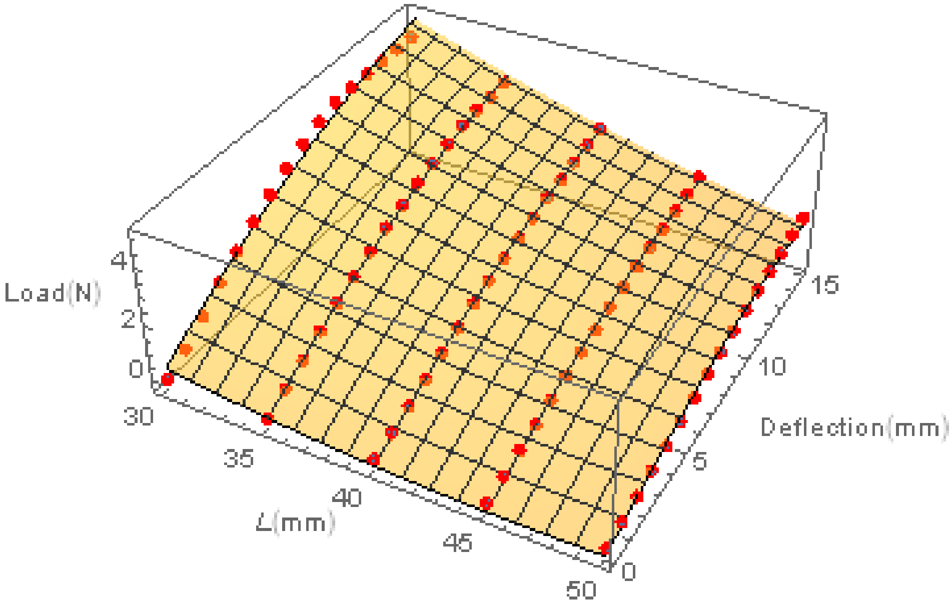

Figure 12. A 3D visualization of the measurement results

The aim of this measurement is to determine the relationship between the bending stiffness and length of needle; thus, sampling the data sets within range showed linear behavior at several lengths (30 mm, 35 mm, 40 mm, 45 mm, 50 mm) are used to acquire the bending stiffness. (Figure 13)

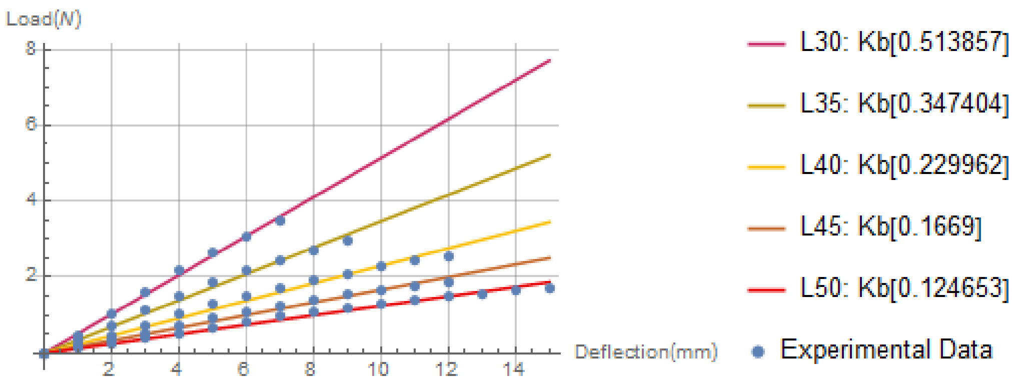

Figure 13. Deflection-Load relationship at several lengths (30 mm, 35 mm, 40 mm, 45 mm, 50 mm)

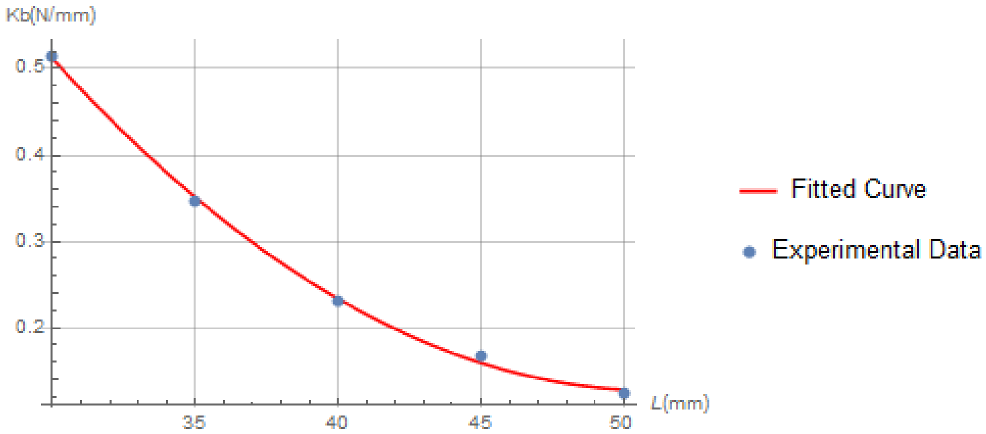

Figure 14. Bending stiffness k_b vs. length of needle L. The red line is fitted to the curve and the blue dots are measurement data.

Measurement data at several application points allows the relationship between the bending stiffness and length of needle to be defined via quadratic polynomial fitting. The measurement results and fitted function are plotted in Figure 14. The bending stiffness is then given by

$$k_b = 0.000865 * L^2 - 0.088388 * L + 2.38463 \qquad (20)$$

where k_b is the bending stiffness and L is the length from the fixed end to the point of the application of force. Equation (20) allows equation (19) to be re-written as

$$f(\theta_0, L, E, I) = \delta_y \qquad (21)$$

where θ_0 is the angle at the free end and L is the perpendicular distance between the needle exit and the pivot plate, E is the material's modulus of elasticity and I is the moment of inertia of the needle's cross-sectional area. We are finally able to define the relationship between the needle tip direction θ_0 and the needle deflection δ_y through equation (21). This relationship can be utilized in the robot future pose estimation to make certain of the needle insertion angle to the target. The calculated result is shown in Figure 15, where L = 40 mm, E = 75 GPa and I = 0.115 mm^4.

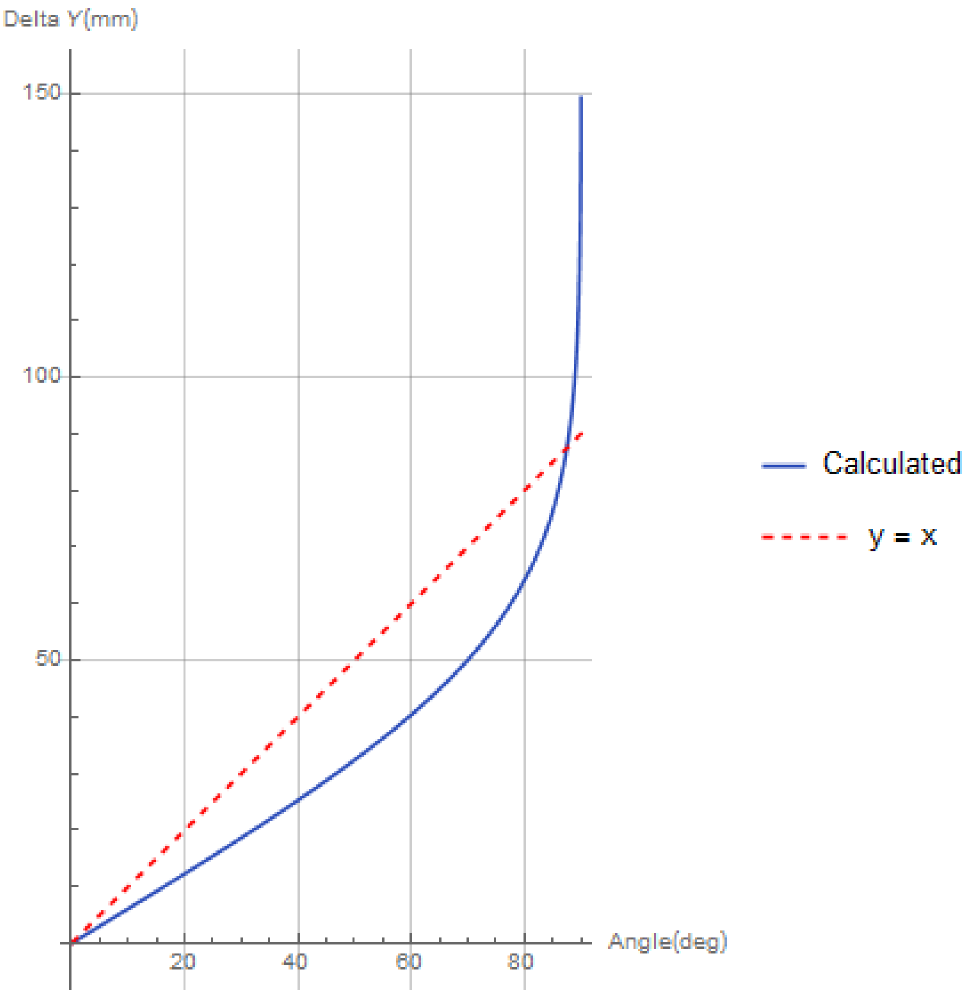

Figure 15. Needle deflection at the pivot point vs. insertion angle at the pivot point, where L = 40 mm, E = 75 GPa and I = 0.115 mm^4.

3.2.4. Define the robot movement direction

Equation (21) is defined in two-dimensional Cartesian coordinates. The direction of the robot's movement should have to be defined for three-dimensional robot control with the estimated movement distance δ_y with respect to the desired angle θ_0. Known geometric information such as the target position and needle pivoting breast plate's hole position from registration allows the easy definition of the plane of motion, and the robot movement direction can be defined on this plane of motion. (Figure 16)

To be specific, directional vector $\overrightarrow{U_{mt}}$ is acquired from minimum distance hole position $\boldsymbol{p}_m$ and target position $\boldsymbol{p}_t$. And directional vector $\overrightarrow{U_{st}}$ is also acquired from selected hole position $\boldsymbol{p}_s$ and target position $\boldsymbol{p}_t$. With these two directional vectors, specific plane can be generated. We use this plane as the plane of motion that robot movement direction for steering $\overrightarrow{U_{MF}}$ is generated. Such constraint of robot motion allows us to find only one solution from equation (21).

By all procedures mentioned in Section 3.2, robot position control for needle steering can be successfully achieved. We utilized the equation to determine the movement of the actuator δ_y to make the desired needle path to the given pivot point to the target point. Because the positions of the pivot point and the target point were given, the angle θ_0 was given. And we knew L from the system dimension and the coordinates of the markers on the robot and the breast plate.

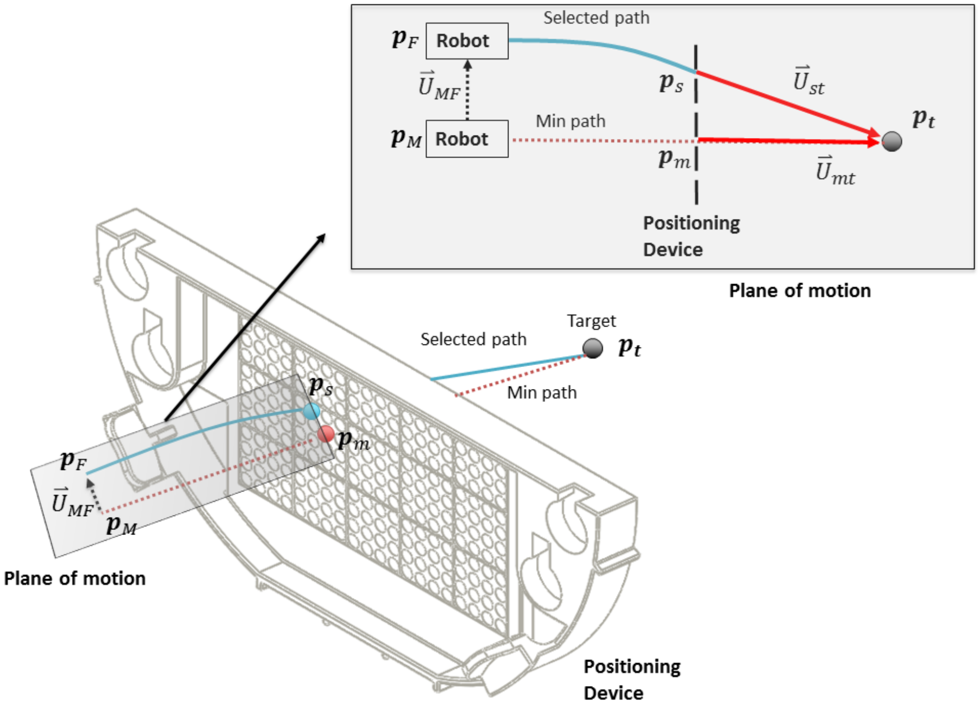

Figure 16. Set plane of motion

3.3. Optimal path selection scenario

The suggested method can offer a detoured possible path to reach the target. This detoured path could provide the opportunity to avoid obstacles located in front of the target. (Figure 17) Furthermore, this method can generate various possible paths to reach the target with the needle pivoting breast plate’s holes. This will allow surgeons to choose the optimal path that can minimize patient trauma.

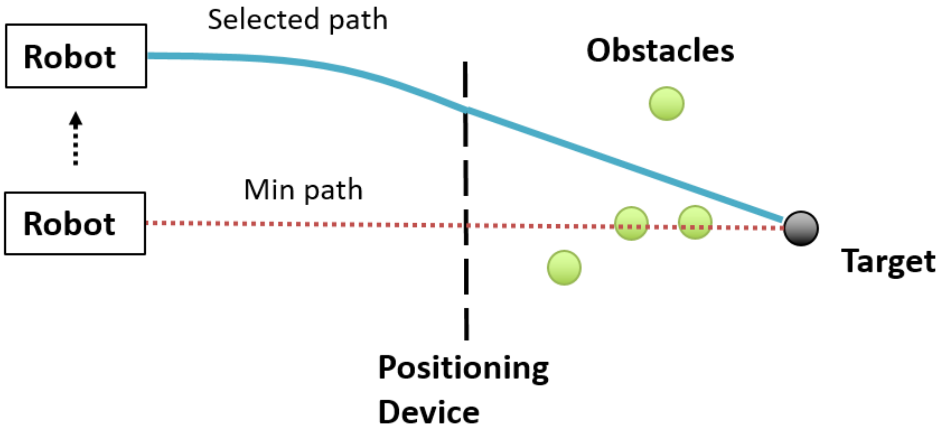

Figure 17. Estimated needle path to reach the target

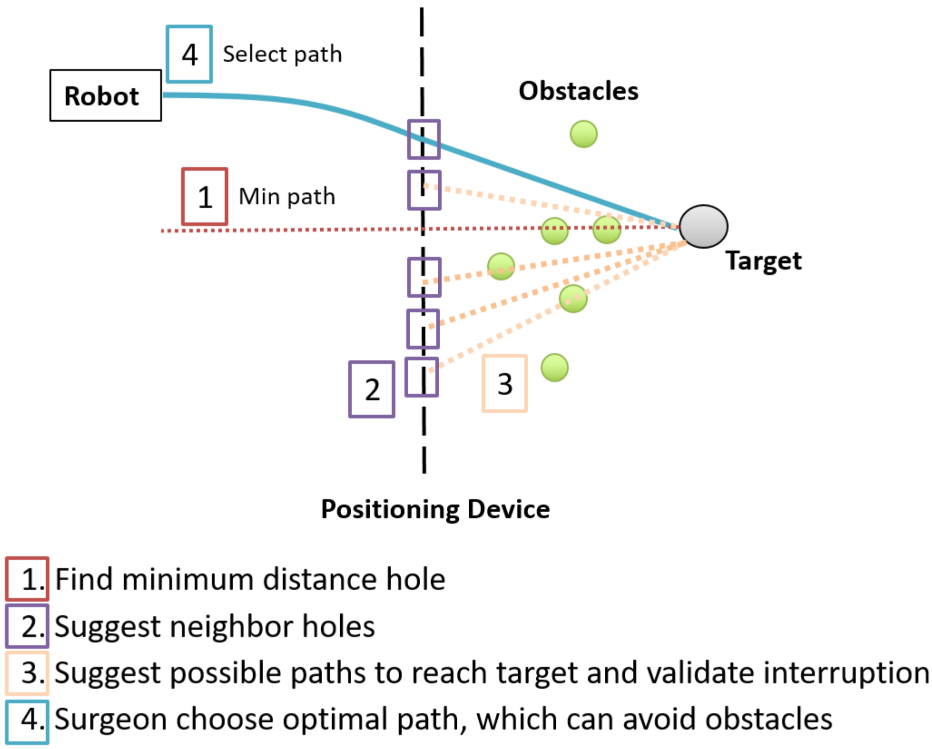

Figure 18. Optimal path selection scenario

The optimal path selection is comprised of the following steps: (1) Find the hole the minimum distance from the target; (2) Suggest neighbor holes to the minimum distance hole; (3) Suggest possible paths to reach the target and validate the interruption; (4) The surgeon chooses the optimal path from the MRI, which allows them to avoid obstacles. (Figure 18.)

Chapter 4. Results

We present the experimental setup used to steer the flexible needle with the proposed method and the targeting results in a laboratory environment in this section.

4.1. *In vitro* Test

4.1.1 Experiment setup

The experimental setup is composed of an MR−guided breast needle intervention robot and an infrared (IR) tracking camera (V120 Slim, OptiTrack, US). In total, eight IR tracking cameras are used in the experiment to track the positions of the target and needle end. (Figure 19) MR fiducial markers to trace the robot position in MRI were also replaced with IR active markers (MTE8600M2, Marktech Optoelctronics, Latham, NY, USA).

An experiment is used to evaluate the needle steering algorithm that is comprised of the following steps: (1) Set the target position; (2) Position the needle tip at the target position; (3) Measure the needle tip position; (4) Compute the targeting error. In total, 45 different paths to the same target position are conducted. All targeting process are conducted via open loop control. The targeting error is computed as follows

$$Targeting\ \ Error = \left\| \boldsymbol{p}_{target} - \boldsymbol{p}_{tip} \right\| \qquad (9)$$

$\boldsymbol{p}_{target}$ is the target position and $\boldsymbol{p}_{tip}$ is the needle tip position.

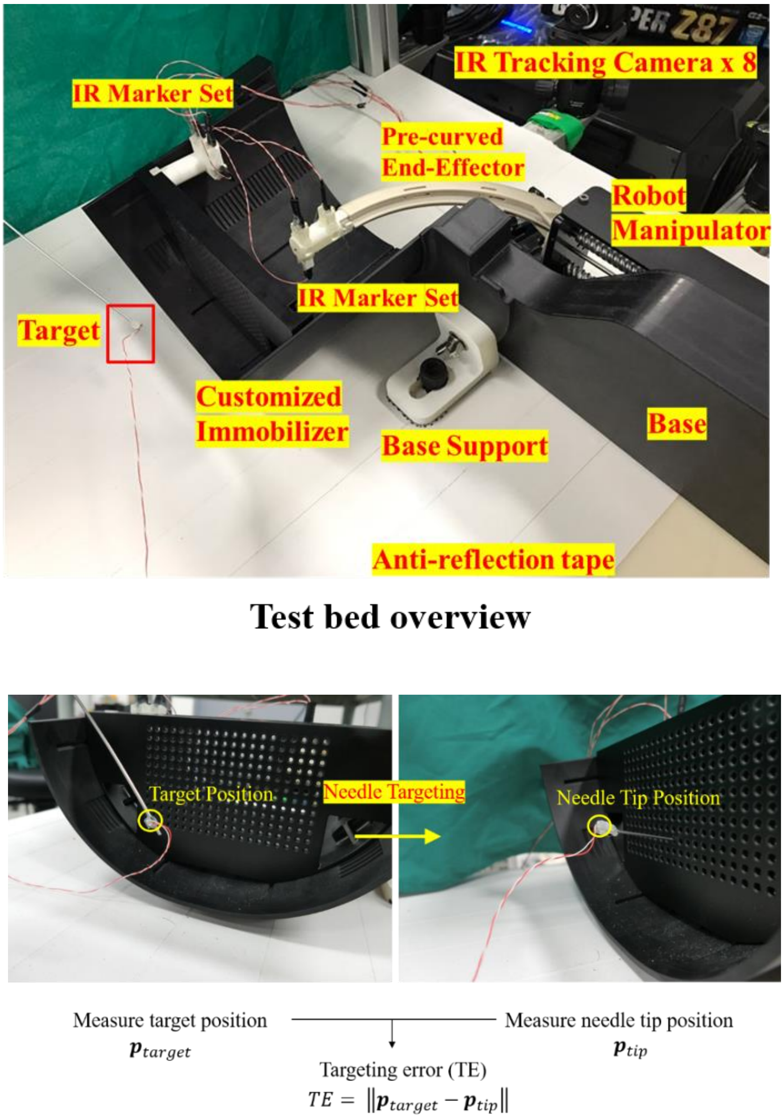

Figure 19. Experimental setup using IR tracking cameras

4.1.2 Target error

The selected holes of the needle pivoting breast plate are shown in Figure 20. We categorized the results as either inside or outside based on its insertion angle.

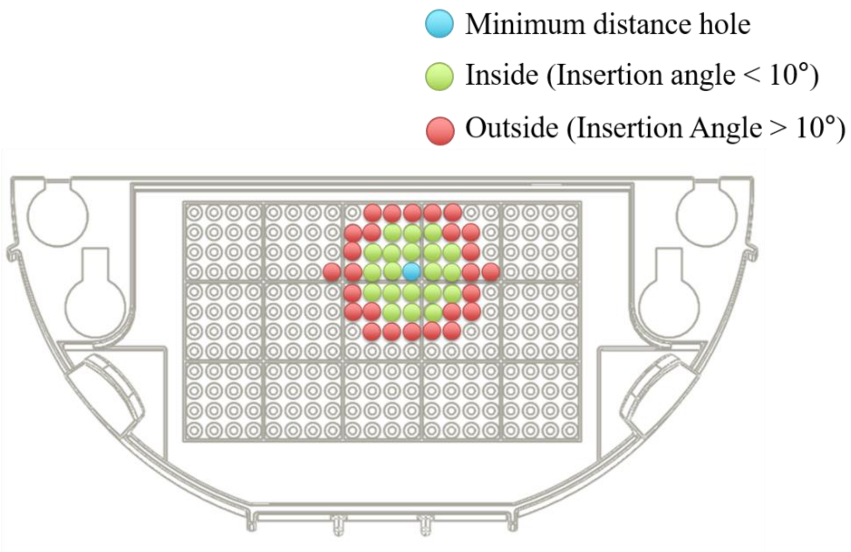

Figure 20. Selected holes for the experiment

The average targeting error and standard deviation of the 45 samples is 4.42 ± 2.58 mm. In the 21 inside paths that have a relatively small insertion angle (less than 10˚), the average targeting error and standard deviation was 3.38 ± 1.86 mm, and in the 24 outside paths that have a relatively large insertion angle (greater than 10˚), the average targeting error and standard deviation is 5.33 ± 2.80 mm. (Figure 21 and Table 2) Figure 22 is a

3D visualization of the targeting results.

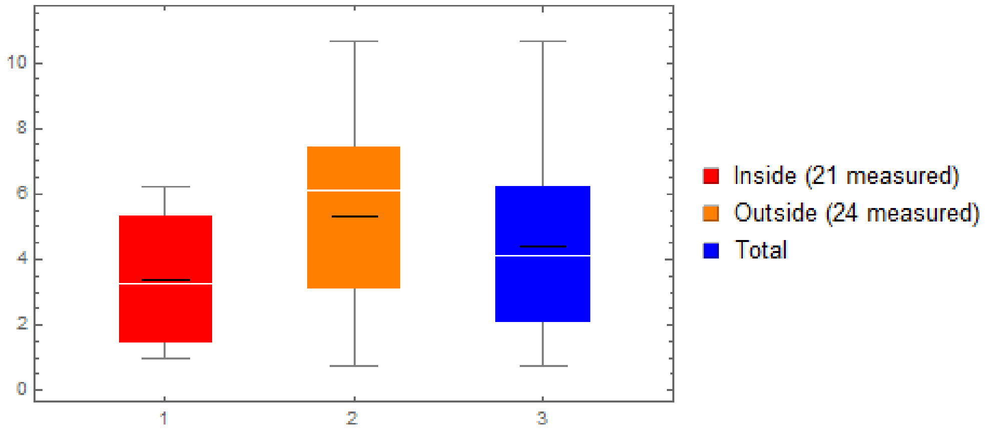

Figure 21. Box whisker chart of the targeting error

In vitro Test	Targeting Error (mm)
21 measured (< 10 ° insertion angle)	3.38 ± 1.86
24 measured (>10 ° insertion angle)	5.33 ± 2.80
45 measured (Total)	4.42 ± 2.58

Table 2. Targeting error results

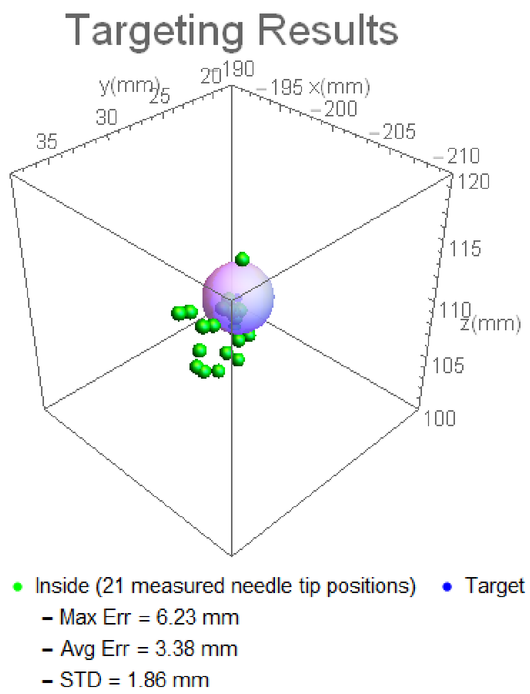
Targeting Results
y(mm)
20
25
30
35
190
195 x(mm)
200
205
210
120
115
110
z(mm)
105
100
Inside (21 measured needle tip positions)
Target
Max Err = 6.23 mm
Avg Err = 3.38 mm
STD = 1.86 mm

(a)

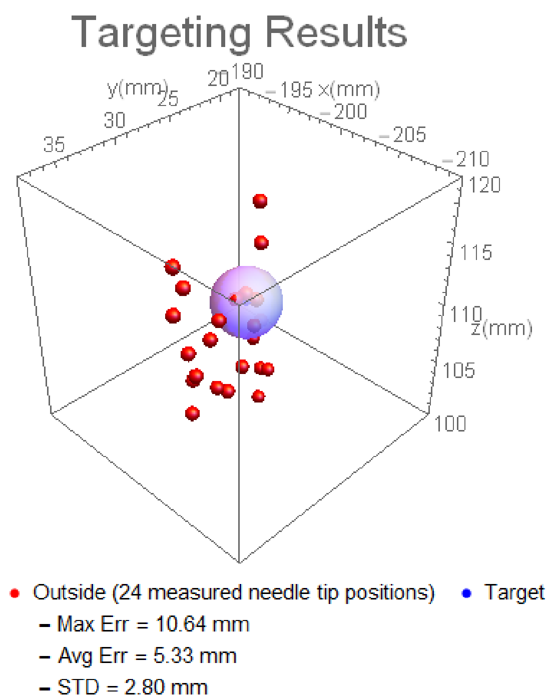
Targeting Results
y(mm)
20
25
30
35
190
195 x(mm)
200
205
210
120
115
110
z(mm)
105
100
Outside (24 measured needle tip positions)
Target
Max Err = 10.64 mm
Avg Err = 5.33 mm
STD = 2.80 mm

(b)

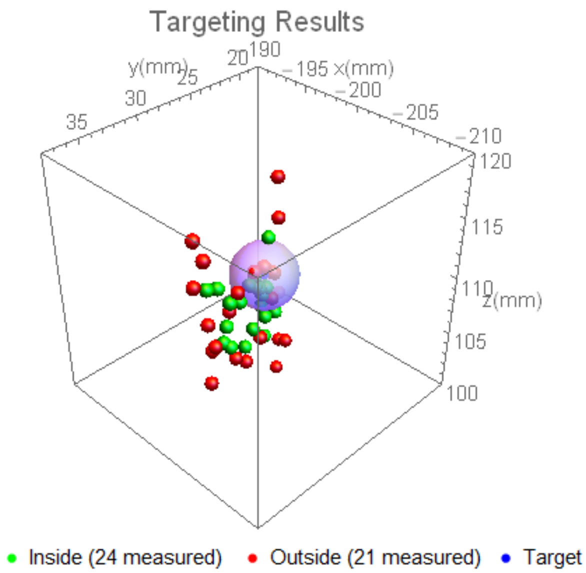

(c)

Figure 22. A 3D visualization of the targeting result; (a) Inside (21 measured needle positions, Insertion angle <10˚); (b) Outside (24 measured needle positions, Insertion angle >10˚); (c) Total (45 samples)

Chapter 5. Discussions

The aim of targeting error was less than 2 mm *in vitro* tests. Unfortunately, the experimental results did not fulfill this goal. Some cases showed a relatively large targeting error of up to 10.64mm. Generally, experimental results show that the targeting error increased in proportion to the insertion angle.

The error can be induced from two factors: (1) the numeric error from the possible non-linear behavior of the needle; (2) the clearance margin of the pivot holes.

The first possible cause of this error is the non-linear behavior of the Nitinol needle, since Nitinol shows non-linear behavior above a certain deformation strain. The large insertion angle meant that the Nitinol needle had a large deflection. When the Nitinol needle was deflected with a large insertion angle, it was possible that it showed non-linear behavior. This non-linear characteristic of the material could induce errors in the needle deflection estimation model based on the behavior of the linear elastic materials. Thus, we need to determine the exact range in which the Nitinol needle works with linear elastic behavior to reduce this error.

The other reason for the error is the gap between the needle and the wall of the pivot hole. (Figure 23) The gap between the needle and wall can cause that the robot' s initial movements are not reflected in the needle tip’ s motion or early reflected in the needle tip’ s motion. This makes the needle steer more than expected or less than expected. A gap can be generated up to 0.8 mm. This is relatively large because the robot’ s general movement is 5-10 mm. Thus, compensating for this gap can reduce the overall targeting error.

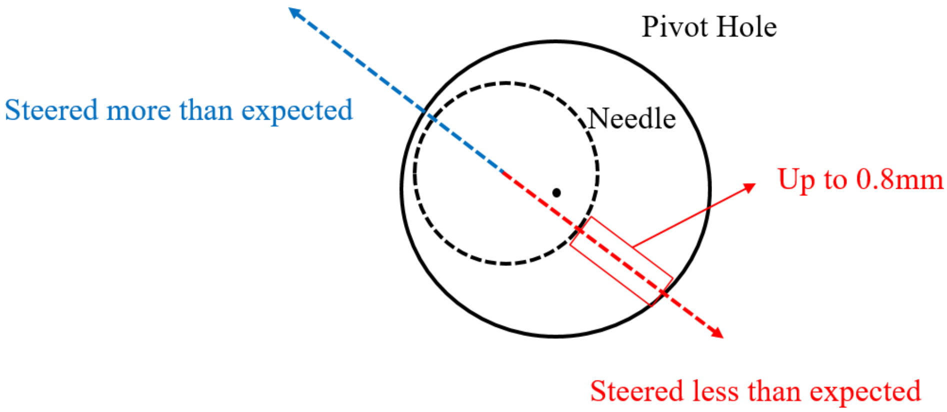

Figure 23. The gap between the needle and wall of the hole

Needle tip placement is controlled by an open loop control, thus targeting results could be improved by additional compensation and feedback control. For example, if the needle insertion direction can be adjusted using MRI feedback (Figure 24 and 25), the needle tip will be placed closer to the target. In addition, compensation for the flexible needle’ s natural deflection inside soft tissue could improve needle tip positioning errors in clinical tests. [13, 14, 15]

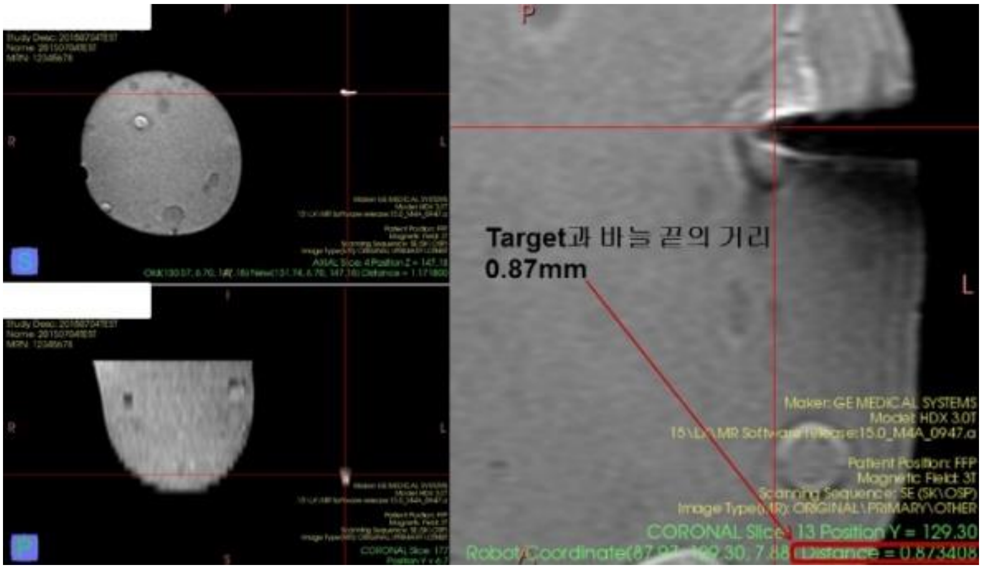

Figure 24. Developed MRI viewer software

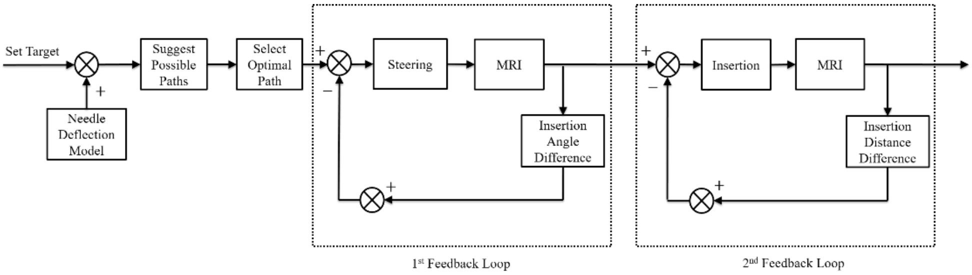

Figure 25. Schematic of the MRI feedback control

The proposed method has several limitations. First, the suggested steering method is not a fully steerable needle. This method just changes the needle tip' s direction to make a detour. Second, the proposed method has a limited range of motion due to the material' s non-linear characteristics and design parameters.

However, the proposed method has the following advantages. This could make various routes to reach the target and minimize the system size increase. In addition, this could be applied to other robotic systems with limited DOFs. These advantages mean that the suggested method will have a positive effect on other robotic breast needle intervention systems.

Bibliography

[1] American Cancer Society (2016) Cancer facts & figures 2016. American Cancer Society, Atlanta

[2] Abolhassani, Niki, Rajni Patel, and Mehrdad Moallem. "Needle insertion into soft tissue: A survey." Medical engineering & physics 29.4 (2007): 413-431.

[3] Podder, T., et al. "Effects of tip geometry of surgical needles: an assessment of force and deflection." IFMBE Proc. Vol. 11. No. 1. 2005.

[4] Lehman, Constance D., et al. "MRI evaluation of the contralateral breast in women with recently diagnosed breast cancer." New England Journal of Medicine 356.13 (2007): 1295-1303.

[5] Kuhl, Christiane K., et al. "MRI for diagnosis of pure ductal carcinoma in situ: a prospective observational study." The Lancet 370.9586 (2007): 485-492.

[6] Yang, Bo, et al. "Design and implementation of a pneumatically-actuated robot for breast biopsy under continuous MRI." Robotics and Automation (ICRA), 2011 IEEE International Conference on. IEEE, 2011.

[7] Yang, Bo, et al. "Design, development, and evaluation of a

master-slave surgical system for breast biopsy under continuous MRI." The International journal of robotics research (2013): 0278364913500365.

[8] Reed, Kyle B., et al. "Robot-assisted needle steering." IEEE Robotics & Automation Magazine 18.4 (2011): 35-46.

[9] Swaney, Philip J., et al. "A flexure-based steerable needle: high curvature with reduced tissue damage." IEEE Transactions on Biomedical Engineering 60.4 (2013): 906-909.

[10] Konh, Bardia, et al. "Design, Development and Evaluation of a Two Way Actuated Steerable Needle." ASME 2015 Conference on Smart Materials, Adaptive Structures and Intelligent Systems. American Society of Mechanical Engineers, 2015.

[11) Ryu, Seok Chang, et al. "Design of an optically controlled MR-compatible active needle." IEEE Transactions on Robotics 31.1 (2015): 1-11.

[12] Shahriari, Navid, et al. "Steering an actuated-tip needle in biological tissue: fusing FBG-sensor data and ultrasound images." (2016).

[13] Webster, Robert J., et al. "Nonholonomic modeling of needle steering." The International Journal of Robotics Research 25.5-6 (2006): 509-525.

[14] Cowan, Noah J., et al. "Robotic needle steering: Design,

modeling, planning, and image guidance." Surgical Robotics. Springer US, 2011. 557−582.

[15] Moreira, Pedro, and Sarthak Misra. "Biomechanics−based curvature estimation for ultrasound−guided flexible needle steering in biological tissues." Annals of biomedical engineering 43.8 (2015): 1716−1726.

[16] Samuel B. Park, J. Kim, K. Lim, C. Yoon, D. Kim, H. Kang, and Yung−Ho Jo, "A Magnetic Resonance Image−Guided Breast Needle Intervention Robot System: Overview and Design Consideration," Int. Journal of Computer Assisted Radiology and Surgery, (Submitted for Review)

[17] Ang, Marcel H., Wang Wei, and Low Teck−Seng. "On the estimation of the large deflection of a cantilever beam." Industrial Electronics, Control, and Instrumentation, 1993. Proceedings of the IECON'93., International Conference on. IEEE, 1993.

[18] Howell, Larry L. Compliant mechanisms. John Wiley & Sons, 2001.

[19] Johnson Matthey Medical Components, http://jmmedical.com/

초 록

MR 유도 바늘 중재시술은 유방의 진단과 치료에서 가장 일반적으로 사용되는 방법이다. 바늘 끝단의 잘못된 도달은 치료의 실패나 오진을 유발할 수 있기 때문에 바늘 끝단의 정확한 목표지점으로의 도달은 시술의 성공여부에 있어 중요하다. 또한, 높은 정밀도를 지니는 바늘 스티어링 로봇 시스템의 개발은 목표지점 앞에 존재하는 중요한 기관들을 회피하여 환자의 후유증을 최소화하기 위해 필요하다. 하지만 강한 자기장의 영향과 협소한 MRI 장비의 보어 크기로 인하여, 고자유도의 로봇 시스템을 구성하는 것은 쉽지 않다. 본 연구는 MR 유도 유방 바늘 중재시술에 효과적으로 활용될 수 있는 MRI 장비의 보어 안의 한정된 공간 안에서 시스템의 크기 증가를 최소화하며 바늘을 스티어링 할 수 있는 전략을 제안한다. 공간적 제약과 병변 앞의 위험 구조물을 회피하기 위한 바늘 끝단 방향의 변화는 피봇 움직임을 통해 수행하였다. 바늘 끝단의 자유도를 증가시키기 위한 바늘 피봇팅 가슴 압착 기구와 피봇된 플렉시블 Nitinol 바늘에서 발생하는 변형을 예측 모델을 고안하였다. 이 예측 모델은 보의 대변형 이론에 근거하였으며, 로봇의 제어에 활용된다. 적외선 위치추적 카메라를 사용한 실험 환경에서 개루프 제어를 통한 바늘의 위치 도달 실험을 수행하여 제안된 방법의 실효성을 검증하였다. 실험으로 측정된 평균 위치 도달 오차와 표준편차는 4.42 ± 2.58 mm 이다.

주요어: MR 유도 유방 바늘 중재시술 로봇, 바늘 피보팅 가슴 압착 플레이트, 바늘 스티어링, 초탄성 플렉시블 바늘, 바늘 변형 예측, 보의 대변형 이론

학 번: 2013-23084